Int J Adv Manuf Technol (2017) 91:2175–2184
DOI 10.1007/s00170-016-9898-0

ORIGINAL ARTICLE

A comparative study of GMAW- and DE-GMAW-based additive manufacturing techniques: thermal behavior of the deposition process for thin-walled parts

Dongqing Yang[1] · **Gang Wang**[1] · **Guangjun Zhang**[1]

Received: 12 October 2016 / Accepted: 18 December 2016 / Published online: 30 December 2016

Abstract The surface temperature of the thin-walled parts deposited by gas metal arc welding (GMAW)- and double-electrode gas meal arc welding (DE-GMAW)-based additive manufacturing (AM) techniques was captured through the infrared thermography technique. The dimensions of the molten pool in the deposition process including length, depth, and width were reduced in different degrees by the bypass arc during the DE-GMAW-based AM. The volume of the molten pool can decrease by about 30% in DE-GMAW under the same deposition rate. The volume of the high-temperature metal for the deposited parts during DE-GMAW-based AM was smaller than that during GMAW-based AM when depositing the high layer. The mean temperature of the deposited parts after the cooling process in DE-GMAW-based AM was lower under the same condition. The bypass arc in DE-GMAW-based AM is conducive to the reduction of the heat accumulation in the deposited thin-walled parts without a corresponding decrease in the deposition rate.

Keywords Additive manufacturing · Double-electrode GMAW · Thermal behavior · Thin-walled part · Infrared thermography

1 Introduction

Additive manufacturing (AM) is an advanced fabrication technology that can make components through layer-by-layer deposition based on the virtual solid models. Due to its advantages of low production costs, short production time and materials saving, AM has become a research hotspot all over the world [1]. Especially with the increasing requirement of industrial production, fabricating metal functional parts directly by additive manufacturing has attracted the attention of many researchers over the recent years [2]. Depending on the energy source utilized in the deposition process, metallic AM technologies can be classified into three groups: laser-based, electron beam-based and welding arc-based [3]. The equipment expenditure and maintenance costs were high in laser and electron beam-based AM. In contrast, the welding arc-based AM has the advantages of low equipment cost and running cost [4]. Moreover, the metal wire was usually served as the deposited raw material in welding arc-based AM processes; thus, it was a cleaner technique with fewer contamination issues, compared with the AM process using powder [5]. Based on the welding methods used in AM, it can be classified into the following groups: gas metal arc welding (GMAW), gas tungsten arc welding (GTAW), and plasma arc welding (PAW). It is generally known that the wire in GMAW acted as a consumable electrode is melted by the welding arc directly. This will lead to high deposition rate in GMAW-based AM. It is more suitable to fabricate the medium and large scale structure metal parts by GMAW based AM.

However, the high deposition rate will bring large heat input into the fabricated part in the deposition process. It has bad effects on the final residual stresses, geometry accuracy, and mechanical properties of the formed parts. Especially during single-pass multi-layer GMAW-based AM, the heat accumulation of the deposited part becomes serious as the deposited height increases [6]. This is a common problem that restricts the development and application of GMAW-based AM technique. Some investigations about the heat accumulation in GMAW-

✉ Guangjun Zhang
zhanggj@hit.edu.cn

[1] State Key Laboratory of Advanced Welding and Joining, Harbin Institute of Technology, West Straight Street 92, Harbin 150001, People's Republic of China

based AM have been explored. Spencer et al. [7] improved the surface finish of the deposited parts by controlling the temperature of the parts through an infrared (IR) thermometer during the GMAW-based AM, but this was at the expense of reduced process efficiency. Zhang et al. [8] presented a wave-controlled short-circuit transfer mode in GMAW-based AM, with some advantages including low heat input, and smooth integration between droplet and weld pool, but the current waveform of welding process must be acquired by experiments in advance. Zhao et al. [6] analyzed the thermal behavior during single-pass multi-layer GMAW-based AM by 3D finite element numerical simulation. The results showed that adopting the same depositing directions can significantly improve the heat diffusion condition of the component. During single-pass multi-layer GMAW-based deposition, Xiong et al. [9, 10] proposed an improved neuron self-learning PSD controller to achieve the desired bead widths of the deposited parts, neglecting the error of the deposition height. Ding et al. [11] proposed an adaptive medial axis transform (MAT) algorithm for GMAW-based additive manufacturing. It can improve geometrical accuracy and save materials more than 27% when fabricating thin-walled structures.

After the summarization of present literatures, the commonly used measures to relieve the heat accumulation are decreasing the welding current, increasing the travel speed, or prolonging the inter-layer cooling time. These will cause lower deposition rate or make the deposition process time-consuming and weaken the advantages of GMAW based AM. In the welding field, the double-electrode gas metal arc welding (DE-GMAW) technique [12–15] was characterized as reducing the heat input into the base metal distinctly through the bypass arc under the same deposition rate. It has been applied into the weld-based additive manufacturing in our previous research [16]. The forming characteristics of multi-layer single-bead deposition by DE-GMAW were investigated and the effect of the bypass current on the forming dimensions and the materials utilization was illustrated in that work.

In order to gain a deeper understanding of DE-GMAW-based AM, it is necessary to investigate the thermal process of this deposition. In this paper, an infrared camera was used to capture the surface temperature of the deposited parts during GMAW- and DE-GMAW-based AM processes. The infrared camera is a non-contact device that detects infrared energy and converts it into an electronic signal, which is then processed to produce a thermal image on a video monitor and perform temperature calculations. In AM researches, Bai et al. [17, 18] utilized the IR imaging for calibrating input material thermal parameters to improve the prediction accuracy of thermal finite element analysis for GMAW-based AM. Rodriguez et al. [19] developed an integrated thermal imaging system in electron beam melting AM with a higher level of feedback that can allow for captured IR images to be analyzed and processed as a means to identify absolute thermal non-uniformity on the part's surface. Farshidianfar et al. [20] established an infrared thermal imaging system to compare the effects of cooling rate and melt pool temperature on the microstructure of 316 L stainless steel produced by laser-based additive manufacturing. Thus, the infrared thermography technique is a convenient, non-contact, non-destructive, and real-time test method for detecting the object temperature in AM process. This paper aims at investigating the influence of the bypass arc on the thermal behavior when depositing the thin-walled parts by DE-GMAW-based AM, compared with the GMAW-based AM.

2 Experimental system

The DE-GMAW-based additive manufacturing system is shown in Fig. 1. The I, I_{bp}, and I_{bm} were wire melting current, bypass current, and base metal current, respectively. DE-GMAW was established by introducing a GTAW torch to form a bypass current loop for the wire melting current. In that way, the base metal current was decoupled from the melting current and the heat input into the base metal was lower with the same wire melting rate. In this work, the Panasonic YD-500FR welding machine with constant voltage mode was the GMAW power supply and the Rilon WS-400 with constant current mode was the bypass arc power supply. During the deposition process, both welding torches were always static and the thin-walled part was fabricated with the movement of the work flat. After the deposition of each layer, the work flat should descend with a certain height. The H08Mn2Si steel wire with 1.2 mm diameter served as a consumable material deposited on the Q235 low-carbon steel plates with dimension of 250 mm × 80 mm × 9.5 mm. The diameter of the tungsten electrode used in the GTAW torch was 3.2 mm. The shielding gas for GMAW torch was Ar (95%) and CO_2 (5%) gas mixture with a constant flow rate of 15 L/min, and the pure Ar gas was supplied for the GTAW torch with 8 L/min flow rate. The relative position of two welding torches and the distance between the torches and substrate were just the same with that in Yang et al. [16].

The main experimental parameters are listed in Table 1. Two groups of experiments for depositing thin-walled parts by DE-GMAW and GMAW have been explored with the same wire feed speed and deposition velocity. The bypass current in the DE-GMAW-based AM was always 80 A, while the GMAW-based AM was without the bypass arc. In the deposition process, the surface temperature of the deposited thin-walled parts was captured by the IR camera, as shown in Fig. 1.

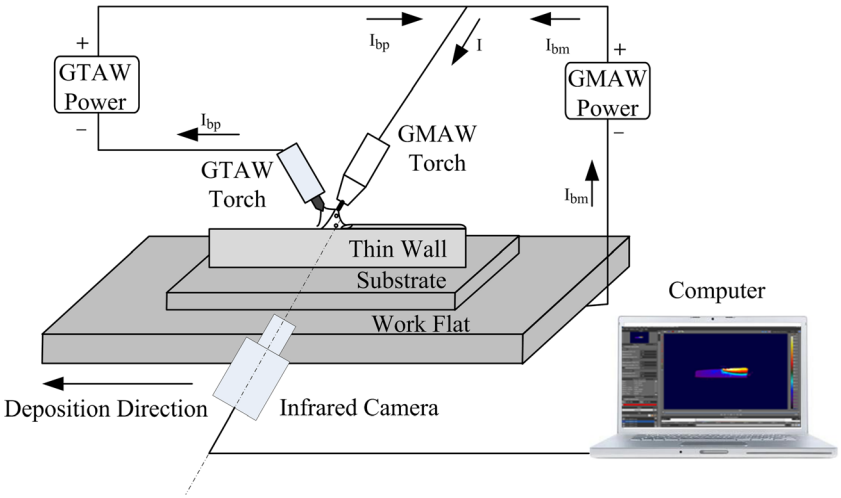

Fig. 1 Schematic diagram of DE-GMAW-based AM system with the IR camera

2.1 IR camera

The IR camera applied in this work was FLIR SC620. The specifications of the interest for this IR camera are provided in Table 2. As shown in Fig. 1, the IR camera was directly facing the plane of the welding torches and the deposited part. For protecting the IR camera lens from the welding spatter, the camera was located at a distance of 1 m from the GMAW torch which provided a resolution of 0.66 mm/pixel. During the deposition process, the surface temperature of the formed parts was recorded by the camera and the data was stored in the related computer for further analysis.

It should be noted that the related parameters setting for the infrared thermography has significant influence on the temperature measurement results. The IR camera worked with a frame rate of 15 Hz. The temperature measurement range of the IR camera was 0–500 or 200–2000 °C. In the metal deposition process, the maximum temperature of the deposited parts was more than 1450 °C (the melting point of the steel) and the temperature measurement range was set as 200–2000 °C. In the cooling process, if the maximum temperature was below 500 °C, the temperature range switched to 0–500 °C. This was because the temperature of some place on the deposited part was likely below the 200 °C after cooling for a period of time. If the larger range was used in this case, the temperature measurement will be inaccuracy. The switching time was shorter than 5 s, and it had a slight effect on the results. The emissivity of the object was also essential for the IR thermography. In this work, after the calibration test using the thermocouple, the emissivity of the deposited parts was set as 0.84, neglecting the influence of the temperature and object's status.

Table 1 Experimental parameters of DE-GMAW-based AM

Parameter	Value
Wire feed speed (m/min)	4.92
Arc voltage (V)	23.5
Deposition velocity (mm/s)	5
Deposited length (mm)	180
Inter-layer cooling time (min)	5
Total number of layers	20

2.2 Error analysis of IR thermography

The temperature measurement accuracy of IR thermography in DE-GMAW-based AM was essential for the subsequent analysis. The typical thermal images of the deposition process and the cooling process captured by the IR camera are shown in Figs. 2a and 2b, respectively. The surface temperature distribution of the deposited part was generally distinct while the temperature of some place in the thin-walled part was not accurate.

In Fig. 2a, the zone under the GMAW torch marked by the red line is worth discussing. Normally, this zone should be molten pool. Thus, the temperature of this place is more than the melting point of the steel at about 1400–1500 °C actually. But, the measured temperature was only about 540 °C. The main reason for this error was the difference of thermal emissivity between the solid and liquid steel. In the calibration test, the measured point by the thermocouple was not in melting point. The calibrated emissivity of the deposited steel part was only suitable for the solid condition. According to Schöpp et al. [21] and Goett et al. [22], the emissivity of the liquid

Table 2 IR camera specifications

Detector type	Uncooled microbolometer
Spectral range (μm)	7.5~13.0
Resolution (pixels)	640 × 480
Frame rate (Hz)	30, 15, 7.5
Standard temperature range (°C)	0~500, 200~2000
Measuring accuracy (%)	±2

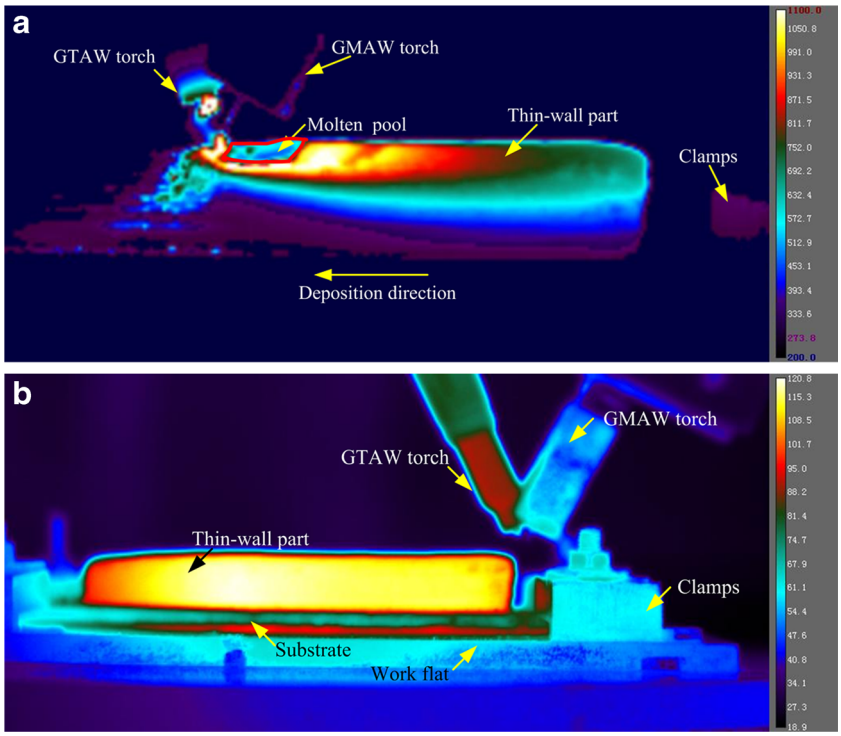

Fig. 2 The typical temperature field distribution of the thin-walled part by the IR camera. **a** In deposition process. **b** In cooling process

S235 steel (a material was similar with the Q235) above the melting point is about 0.1–0.3, decreasing with an increase of the temperature. In this work, the emissivity was set as 0.84, much larger than the one of liquid steel. According to the Stefan-Boltzmann law, the measured temperature is inversely proportional to the emissivity. It naturally led to the lower measured temperature in molten pool. If the emissivity was set as 0.2, the temperature of the zone encompassed by the red line in Fig. 2a was about 1455 °C. This result was more correct and approximated well to the real one. Therefore, the measurement error in the molten pool was due to the inaccuracy of the emissivity. Furthermore, the temperature of the zone ahead of molten pool along the deposition direction was also incorrect due to the disturbance from welding arc and fume. Although the measurement error has some influence on the thermal analysis for DE-GMAW-based AM, the majority of the data calculated through the IR thermography was reliable and accurate. Particularly, after the extinction of welding arc, the molten pool cooled and solidified. The temperature measurement in this period will not get affected by the welding arc and the inaccuracy of the emissivity. As shown in Fig. 2b, the surface temperature of the deposited part in cooling process is clear and accurate. Therefore, for the convenience of the calculation, the emissivity was always set as 0.84 in this work.

2.3 Extraction of molten pool

As explained in Section 2.2, the great difference in emissivity of the thin-walled part between the solid state and liquid state will lead to the significant error in the temperature measurement of the molten pool. The calculated temperature of molten pool using the emissivity of solid state was far lower than the melting point of the steel. In this way, the temperature of the molten pool was also far lower than the temperature of the

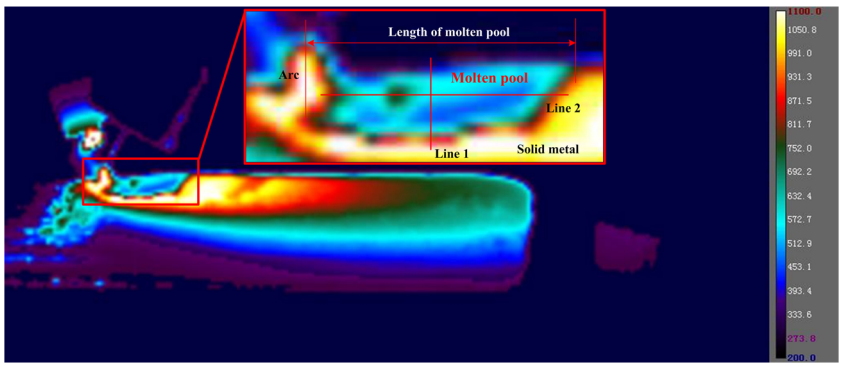

Fig. 3 The temperature distribution of molten pool in the deposition process

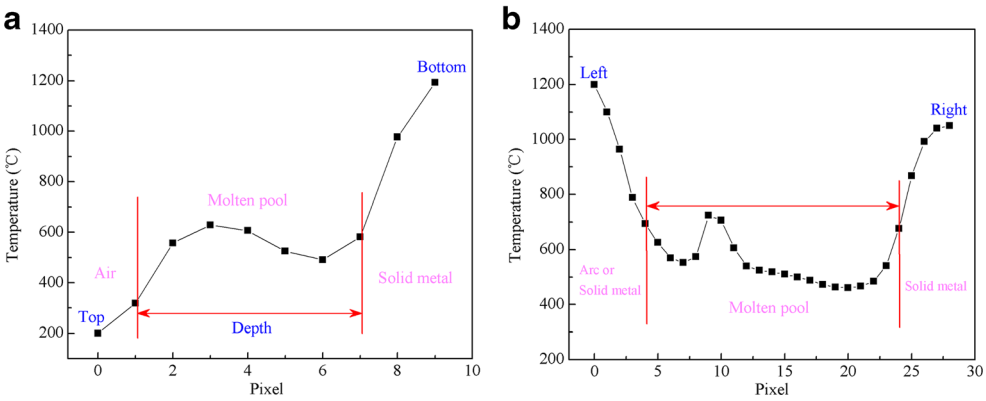

Fig. 4 The temperature distribution of the *marked lines* in Fig. 3. **a** Line 1. **b** Line 2

solid metal nearby the molten pool. Therefore, this measurement error can supply an approach to extract the profile of the molten pool in the deposition process. As illustrated in Fig. 3, the temperature distribution picture of the molten pool and its vicinity was enlarged and the boundary of the molten pool was distinct. The temperature data of this area can be extracted by the included FLIR software ResearchIR, and accordingly, the information of the molten pool will be acquired. The temperature distribution of two red marked lines at the molten pool, in the vertical and horizontal direction, respectively, is presented in Fig. 4.

As shown in Fig. 4a, the horizontal coordinate denotes the distance from the top to the point of line 1, and the vertical coordinate shows the corresponding temperature. According to the temperature distribution of line 1, the depth of molten pool can be figured out. There were two mutations in temperature as illustrated in Fig. 4a. The top of line 1 was in the air; thus, the temperature of pixel 0 was the lower threshold of the measurement range of about 200 °C. From the air to the molten pool, the temperature rose very fast. Pixel 1 was the first mutation and can be seen as the boundary of the air and molten pool. Due to the great difference in emissivity between the solid and liquid steel, the temperature of molten pool measured by the IR thermography using the solid steel's emissivity was far lower than the melting point with enormous error. The metal nearby the molten pool should be solid with high temperature close to the melting point. In Fig. 4a, the temperature of pixel 7 was only 580 °C, while the temperature was 1000 °C on pixel 8 and then reached more than 1200 °C on pixel 9. It was exactly in accordance with the previous analysis. Therefore, pixel 7 was the other mutations and can be seen as the boundary of the molten pool and solid metal. Accordingly, the distance between the boundaries was the depth of the molten pool. At this moment, the depth of the molten pool was 7 pixels, approximately equal to 4.6 mm in this work.

In Fig. 4b, the temperature distribution of line 2 was similar with that in line 1. Using the same method, the left and right boundaries of line 2 also can be achieved. But, the difference of the two boundaries was not the length of the molten pool. As illustrated in Fig. 3, the length of the molten pool was the horizontal distance of the left-most and right-most feature points. Through the ResearchIR software, the area of the molten pool marked by red line in Fig. 2a was also obtained.

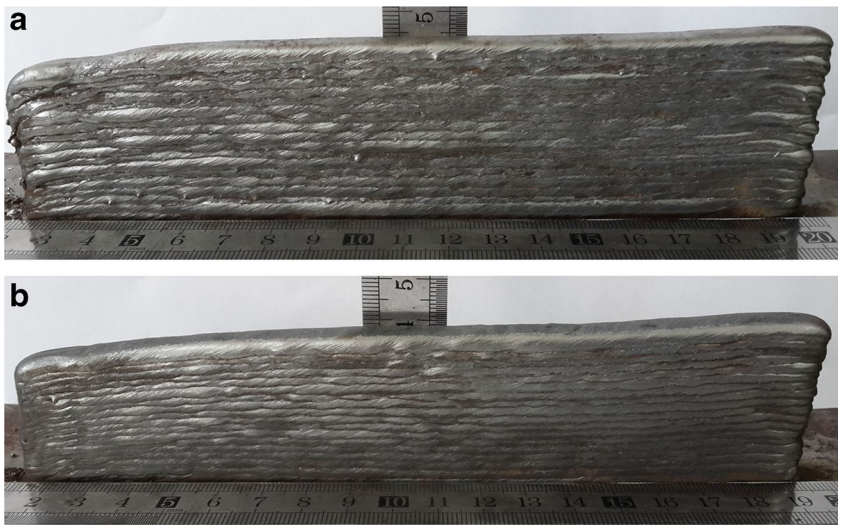

Fig. 5 The final thin-walled parts deposited by **a** DE-GMAW and **b** GMAW

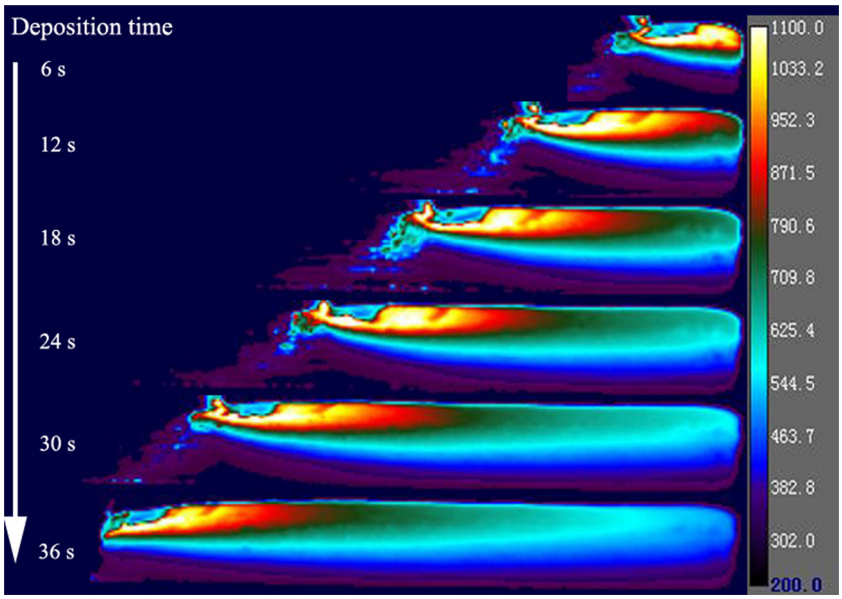

Fig. 6 The evolution of molten pool in the tenth layer deposition during the DE-GMAW-based AM process

3 Results and discussion

The final thin-walled parts deposited by DE-GMAW and GMAW are shown in Fig. 5. Generally speaking, the forming appearance of the parts was good without the overflowing and collapsing of welding pool. The forming characteristics of the deposited parts were in accordance with the results in our previous work [16]. In this section, the molten pool, the high-temperature metal, and the mean temperature of the deposited parts will be discussed.

3.1 Molten pool

The molten pool in the deposition process was crucial. The evolution of molten pool within the tenth layer deposition during DE-GMAW-based AM is shown in Fig. 6. As deposition time goes on, the molten pool has little change. Only at the last moment of the deposition process, the molten pool has a tendency to flow down due to the low arc, extinguishing end in the same deposition direction according to Xiong et al. [23]. The information of the molten pool within a certain layer has been extracted for 6 to 30 s in the deposition process.

The typical molten pool in the deposition process during the DE-GMAW- and GMAW-based AM is shown in Fig. 7. This moment was in the middle of the 20th layer deposition in both AM processes. It was obvious that the molten pool of the GMAW-based deposition was larger. The dimensions and area of the molten pool in the GMAW-based AM and DE-GMAW-based AM are shown in Fig. 8 after data processing. In order to extract the molten pool accurately, the results in the deposition process from the 5th layer to 20th layer were used to

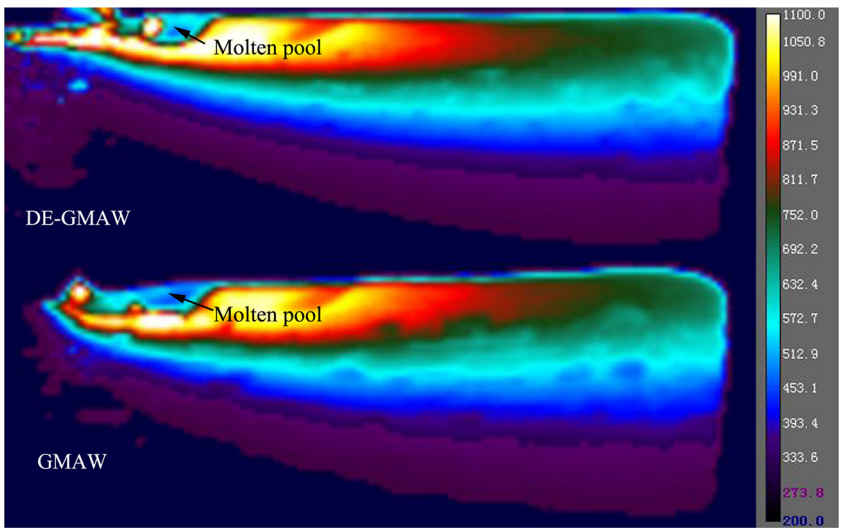

Fig. 7 The molten pool in the deposition process during DE-GMAW- and GMAW-based AM

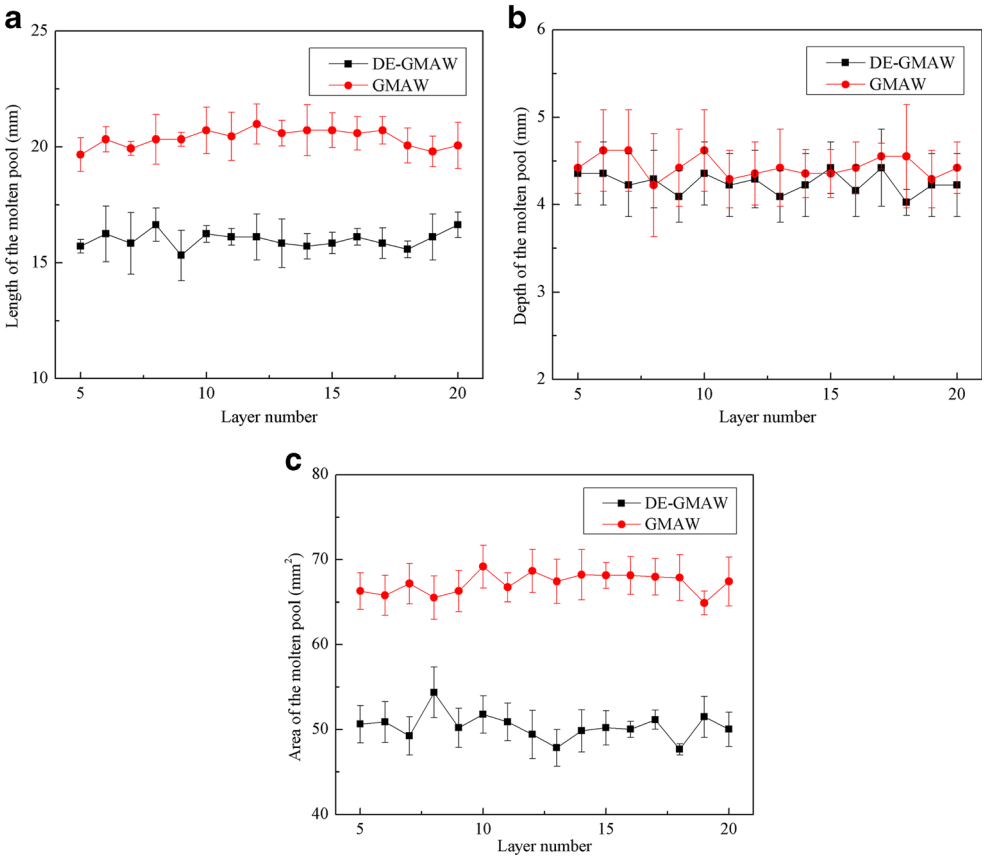

Fig. 8 The information of the molten pool in DE-GMAW- and GMAW-based AM. **a** Length of the molten pool. **b** Depth of the molten pool. **c** Area of the molten pool

analyze the molten pool. In Fig. 8, the length, depth, and area of the molten pool showed a little change in different layers during the DE-GMAW-based AM and GMAW-based AM. This illustrated that after the fifth layer deposition, the process was stable. The molten pool in DE-GMAW-based AM was about 20% shorter than that in GMAW-based AM. The depth of the molten pool in GMAW-based AM was 4.43 mm, while it was 4.25 mm in DE-GMAW process. The difference of the depth in both deposition processes was slight. The area of the molten pool in DE-GMAW was about 25% compared to that in GMAW process.

According to the cross section of the final parts, the width of the thin-walled part deposited by GMAW was 9.12 mm, while it was 8.0 mm in DE-GMAW-based AM. It can be viewed as the width of the molten pool. Therefore, the geometry dimensions of the molten pool in DE-GMAW-based process were all lesser than those in GMAW-based process. Obviously, the volume of the molten pool was smaller in DE-GMAW-based AM. Assuming the molten pool was semi-ellipsoid, the volume of liquid metal decreased by about 30% in DE-GMAW-based AM. The liquid metal in the molten pool was composed of the deposited metal from the wire and the melting base metal. In this work, the deposited metal per unit time was almost the same in the two deposition processes due to the same wire feed speed and deposition velocity. Thus, the melting base metal in GMAW-based AM was more than

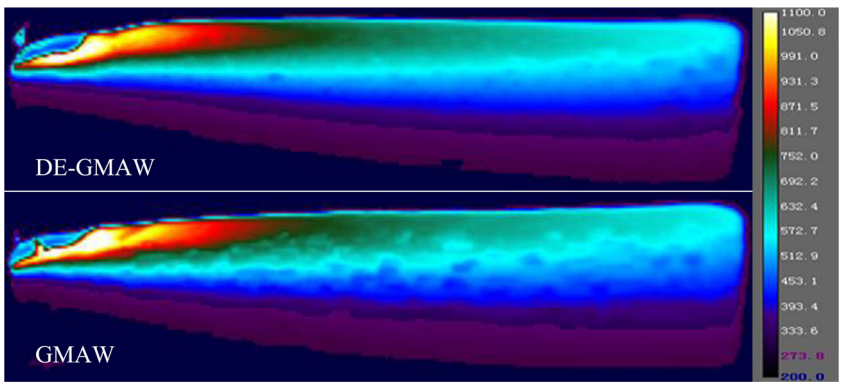

Fig. 9 The surface temperature distribution of the thin-walled part after the 20th layer deposition in DE-GMAW- and GMAW-based AM

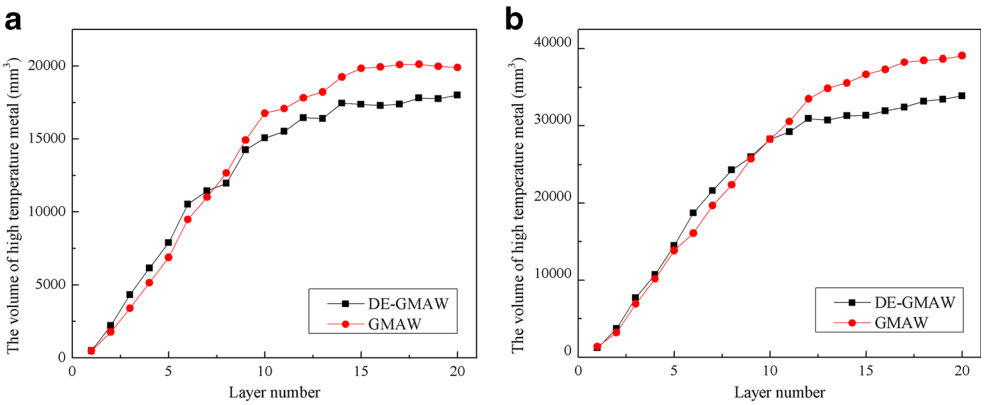

Fig. 10 The volume of high-temperature metal in thin-walled part after deposition of each layer. **a** Above 500 °C. **b** Above 300 °C

that in DE-GMAW deposition process. It indicated that with the bypass arc, the heat input into the deposited parts in DE-GMAW was lesser than that in GMAW-based AM.

3.2 The volume of high-temperature metal

According to the thermal images, the surface temperature distribution of the thin-walled part was apparent. The volume of the high-temperature metal in the deposited part after deposition of each layer can reflect the heat accumulation of the whole part. As shown in Fig. 9, the high-temperature area of the thin-walled parts can be obtained directly by the software ResearchIR. With a simplified calculation, the volume of the high-temperature metal was equal to the product of the width and the high-temperature area. The results of the high-temperature metal are shown in Fig. 10. In both deposition processes, the volume of the high-temperature metal increased with the rising layer number at the first 12 layers and then tended towards stability. This indicated that the heat accumulation of the deposited parts was increasingly serious as the deposited height increased. For the condition above 500 °C in Fig. 10a, in the first ten layers, the volume of the high-temperature metal in both deposition processes was nearly the same. In the last ten layers, the volume of the high-temperature metal in DE-GMAW-based AM was apparently smaller than that in GMAW-based AM. For the condition above 300 °C, the result was similar with this.

The proposed reason for the results is the different heat conduction conditions in the two AM processes. In GMAW-based AM, the width of the thin-walled part was larger than that in DE-GMAW-based AM. Therefore, the heat conduction to the substrate was worse in DE-GMAW-based AM, especially at the first several layers with lower deposition height. Although the heat input entering into the deposited part during the DE-GMAW process was lower, the volume of the high-temperature metal was not small than the one in GMAW-based process. As the deposition height increased, the heat conduction to the substrate became more difficult in both processes. For DE-GMAW-based AM, the lower heat input resulted into the smaller volume of the high-temperature metal. Thus, the volume of the high-temperature metal in DE-GMAW reduced about 10% in the higher deposition layers, compared to the GMAW-based AM.

3.3 The mean temperature

The temperature distribution of the thin-walled part after the cooling process is important for the deposition of the next layer in AM process. When the deposition of the 20th layer was complete, the temperature distribution of the thin-walled part after cooling for 5 min in both AM processes is shown in

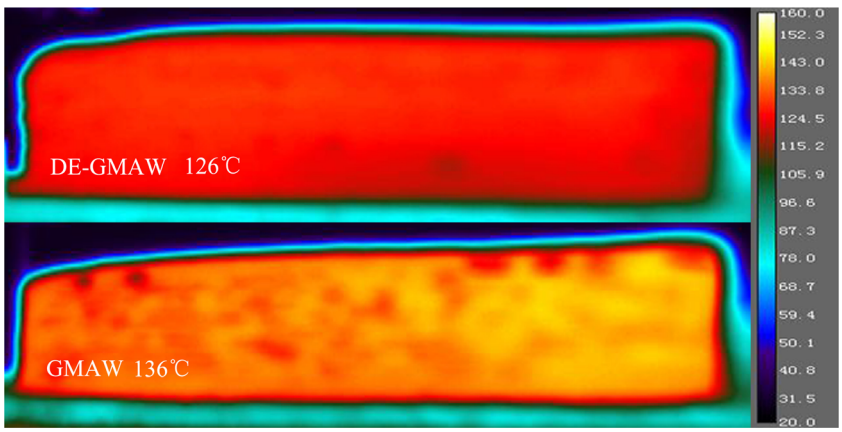

Fig. 11 The temperature distribution of the final thin-walled parts after cooling for 5 min during DE-GMAW- and GMAW-based AM

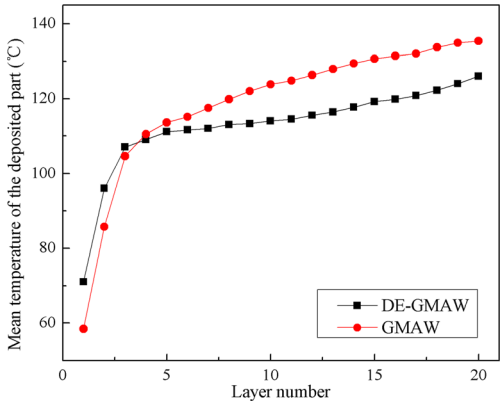

Fig. 12 The mean temperature of the thin-walled part after cooling

Fig. 11. The mean temperature was 126 °C in DE-GMAW-based AM, while it was 136 °C in GMAW-based AM. The mean temperature of the thin-walled part after cooling in each layer is shown in Fig. 12. As the layer number increased, the mean temperature of the deposited parts raised gradually in both AM processes. At the first three layers, the mean temperature in the DE-GMAW process was higher than that in the GMAW process. At the subsequent layers, the mean temperature became lower in DE-GMAW-based AM. The reason for this result was similar with the one for the volume of the high-temperature metal in Section 3.2. At the last ten layers, the mean temperature of the deposited part can drop more than 10 °C in DE-GMAW-based AM, compared to the GMAW-based AM with the same condition. Therefore, the bypass arc in DE-GMAW-based AM has a remarkable influence on the thermal behavior when depositing the thin-walled parts. It contributes to reducing the heat accumulation of the deposited parts.

3.4 Future work

According to the above discussion on the thermal behavior of DE-GMAW- and GMAW-based AM processes, the bypass arc can reduce the heat input into the deposited thin-walled part with the same deposition rate in DE-GMAW-based AM. Meanwhile, the bypass arc also can influence the deposited dimensions regularly in the DE-GMAW-based AM process [16]. The advantages of this AM technology should be adopted to achieve high-quality metal parts with a high-efficiency deposition process. There are still some contents worthy of further study. In our later work, based on the research of the thermal behavior for the DE-GMAW-based AM process, the influence of the bypass arc on the microstructure and mechanical properties of the deposited metal part such as aluminum alloy and high-strength steel needs further researches. It is meaningful to fabricate metal parts with good mechanical properties and microstructure through adjusting the bypass current if possible. Moreover, in order to help the DE-GMAW-based AM to become an industry-acceptable and stable process, it is necessary to monitor and control this deposition process in the future.

4 Conclusions

Based on the analysis and discussion above, the conclusions can be obtained as follows:

1. The information of molten pool in the deposition process for thin-walled part can be extracted from the infrared image. The dimensions and volume of molten pool in DE-GMAW-based AM were smaller than those in GMAW-based AM under the same deposition rate.
2. The volume of the high-temperature metal in the deposition process was smaller in the DE-GMAW-based AM, especially during the deposition of high layer.
3. The mean temperature of the deposited part after the cooling process of each layer was lower in the DE-GMAW-based AM, compared with the GMAW-based AM under the same condition.
4. The bypass arc in DE-GMAW-based AM can reduce the heat input into the deposited part with the same deposition rate, compared with the GMAW-based AM.

Acknowledgements This work was supported by the National Natural Science Foundation of China (No 51575133).

References

1. Huang SH, Liu P, Mokasdar A, Hou L (2013) Additive manufacturing and its societal impact: a literature review. Int J Adv Manuf Technol 67:1191–1203
2. Tapia G, Elwany A (2014) A review on process monitoring and control in metal-based additive manufacturing. ASME J Manuf Sci Eng 136:1–10
3. Ding DH, Pan ZX, Cuiuri D, Li HJ (2015) Wire-feed additive manufacturing of metal components: technologies, developments and future interests. Int J Adv Manuf Technol 81:465–481
4. Baufeld B, Brandl E, Biest O (2011) Wire based additive layer manufacturing: comparison of microstructure and mechanical properties of Ti–6Al–4V components fabricated by laser-beam deposition and shaped metal deposition. J Mater Process Technol 211:1146–1158
5. Martina F, Mehnenb J, Williams SW, Colegrove P, Wanga F (2012) Investigation of the benefits of plasma deposition for the additive layer manufacture of Ti-6Al-4V. J Mater Process Technol 212:1377–1386
6. Zhao HH, Zhang GJ, Yin ZQ, Wu L (2011) A 3D dynamic analysis of thermal behavior during single-pass multi-layer weld-based rapid prototyping. J Mater Process Technol 211:488–495
7. Spencer JD, Dickens PM, Wykes CM (1998) Rapid prototyping of metal parts by three-dimensional welding. Proc Inst Mech Eng Part B-J Eng Manuf 212:175–182
8. Zhang YM, Chen YW, Li PJ, Male AT (2003) Weld deposition-based rapid prototyping: a preliminary study. J Mater Process Technol 135:347–357

9. Xiong J, Zhang GJ, Qiu ZL, Li YZ (2013) Vision-sensing and bead width control of a single-bead multi-layer part: material and energy savings in GMAW-based rapid manufacturing. J Clean Prod 41:82–88
10. Xiong J, Yin ZQ, Zhang WH (2016) Closed-loop control of variable layer width for thin-walled parts in wire and arc additive manufacturing. J Mater Process Technol 233:100–106
11. Ding DH, Pan ZX, Cuiuri D, Li HJ, Larkin N (2016) Adaptive path planning for wire-feed additive manufacturing using medial axis transformation. J Clean Prod 133:942–952
12. Zhang YM, Jiang M, Lu W (2004) Double electrodes improve GMAW heat input control. Weld J 83(11):39–41
13. Li KH, Chen JS, Zhang YM (2007) Double-electrode GMAW process and control. Weld J 86(8):231s–237s
14. Li KH, Zhang YM (2008) Consumable double-electrode GMAW part I: the process. Weld J 87(1):11s–17s
15. Li KH, Zhang YM (2008) Consumable double-electrode GMAW part II: monitoring, modeling, and control. Weld J 87(2):44s–50s
16. Yang DQ, He CJ, Zhang GJ (2016) Forming characteristics of thin-wall steel parts by double electrode GMAW based additive manufacturing. J Mater Process Technol 227:153–160
17. Bai XW, Zhang HO, Wang GL (2013) Improving prediction accuracy of thermal analysis for weld-based additive manufacturing by calibrating input parameters using IR imaging. Int J Adv Manuf Technol 69:1087–1095
18. Bai XW, Zhang HO, Wang GL (2015) Modeling of the moving induction heating used as secondary heat source in weld-based additive manufacturing. Int J Adv Manuf Technol 77:717–727
19. Rodriguez E, Mireles J, Terrazas CA, Espalin D (2015) Approximation of absolute surface temperature measurements of powder bed fusion additive manufacturing technology using in situ infrared thermography. Additive Manufacturing 5:31–39
20. Farshidianfar MH, Khajepour A, Gerlich AP (2016) Effect of real-time cooling rate on microstructure in laser additive manufacturing. J Mater Process Technol 231:468–478
21. Schöpp H, Sperl A, Kozakov R, Gött G, Uhrlandt D, Wilhelm G (2012) Temperature and emissivity determination of liquid steel S235. J Phys D Appl Phys 45:235203 (9pp)
22. Goett G, Kozakov R, Uhrlandt D, Schoepp H, Sperl A (2013) Emissivity and temperature determination on steel above the melting point. Weld World 57:595–602
23. Xiong J, Yin ZQ, Zhang WH (2016) Forming appearance control of arc striking and extinguishing area in multi-layer single-pass GMAW-based additive manufacturing. Int J Adv Manuf Technol 87:579–586